ELSEVIER

Contents lists available at ScienceDirect

Molecular and Cellular Endocrinology

journal homepage: www.elsevier.com/locate/mce





TXNIP overexpression in mice enhances streptozotocin-induced diabetes severity

Marlon R. Schneider^a, Silja Zettler^b, Birgit Rathkolb^{b,c}, Maik Dahlhoff^{d,*}

- ^a Institute of Veterinary Physiology, Faculty of Veterinary Medicine, University of Leipzig, Leipzig, Germany
- ^b Institute of Molecular Animal Breeding and Biotechnology, Gene Center, LMU München, Munich, Germany
- ^c German Mouse Clinic, Institute of Experimental Genetics, Helmholtz Zentrum München, Neuherberg, Germany
- d Institute of in vivo and in vitro Models, Department of Biomedical Sciences, University of Veterinary Medicine Vienna, Vienna, Austria

ARTICLE INFO

Keywords: TXNIP Diabetes mellitus Blood glucose Mouse model Diet-induced obesity Apoptosis

ABSTRACT

Thioredoxin-interacting protein (TXNIP) is a key player in the endocrine pancreas; it induces beta cell apoptosis, such that TXNIP deficiency promotes beta cell survival. To study its function in more detail, we generated transgenic mice with ubiquitous overexpression of TXNIP. CBA^{TXNIP/+} mice were investigated under basal conditions and after being challenged in diet-induced obesity (DIO) and streptozotocin-induced type 1 diabetes mellitus (T1DM) models. TXNIP overexpression caused no effect in the DIO model, contrasting to the already reported TXNIP-deficient mice. However, in the T1DM background, CBA^{TXNIP/+} animals showed significantly enhanced blood glucose and increased glucose levels in a glucose tolerance test. Finally, the beta cell mass of CBA^{TXNIP/+} transgenic animals in the T1DM model was significantly reduced compared to control littermates. Our study demonstrates that overexpression of TXNIP doesn't affect blood glucose parameters under basal conditions. However, overexpression of TXNIP in a T1DM model enhances the severity of the disease.

1. Introduction

Thioredoxin-interacting protein (TXNIP) was originally identified in HL-60 cells and initially named vitamin D3 upregulated protein (VDUP1) (K. S. Chen and DeLuca, 1994). TXNIP has two redox active cysteine residues, which may bind thioredoxin 1 and 2 (TRX1, TRX2) and downregulate their expression (Nishiyama et al., 1999). Together, TRX1 and TXNIP can form the so-called "redoxome" complexes, which are redox-sensitive signaling complexes that regulate the cellular redox status (Yoshihara et al., 2014). TXNIP is present in the cytoplasm and can translocate into mitochondria to bind TRX2 (Junn et al., 2000; Saxena et al., 2010), which causes an activation of apoptosis signal-regulating kinase 1 (ASK1) and triggers apoptosis (Lu and Holmgren, 2012). Accordingly, TRX1 inhibition increased reactive oxygen species (ROS) and the resulting oxidative stress induced cell cycle arrest or apoptosis (Ye et al., 2017). Additionally, through the interaction with TRX, TXNIP is also involved in NACHT, LRR and PYD domains-containing protein 3 (NLRP3) mediated inflammation reaction (Zhou et al., 2010).

In diabetic cardiomyopathies, an increased expression of TXNIP was detected, whereby a reduction of TXNIP decreased apoptosis and

improved survival of cardiomyocytes (Chen et al., 2009). TXNIP-deficient mice show a significant reduction of killer cell number and activity, while at the same time hepatocellular carcinomas develop at a rate of 40% (Lee et al., 2005; Sheth et al., 2006). TXNIP was identified as a tumor suppressor in a variety of cancer types, including liver, pancreatic, breast, lung, and thyroid cancers. The tumor suppressor function makes TXNIP an interesting candidate for innovative cancer therapies (Li et al., 2017).

An influence of TXNIP on pancreatic beta cells was demonstrated in various rodent disease models (Shalev, 2014). TXNIP-deficient mice have an increased beta cell mass and are protected from streptozotocin-induced beta cell destruction and thus from diabetes (Chen et al., 2008a). Notably, beta cells show an increased susceptibility for oxidative stress (Shalev, 2014), and a link between beta cell apoptosis and TXNIP overexpression was established (Minn et al., 2005a; Minn et al., 2005b). TXNIP may also downregulate the insulin production of beta cells, insulin in turn acting as a negative feedback signal for TXNIP expression (Shaked et al., 2009; Xu et al., 2013). On the other hand, a dependency between TXNIP expression and plasma glucose concentration was found, and an increase of TXNIP expression was observed in type 1 diabetes mellitus (T1DM) with hyperinsulinemia and hyperglycemia (Chen et al., 2008b). TXNIP limits glucose uptake by

^{*} Corresponding author. University of Veterinary Medicine Vienna, Institute of *in vivo* and *in vitro* Models, Veterinarplatz 1, 1210, Vienna, Austria. *E-mail address:* Maik.Dahlhoff@vetmeduni.ac.at (M. Dahlhoff).

Abbreviations		LDL:	low-density lipoprotein
		mRNA	messenger ribonucleic acid
ALT	alanine aminotransferase	NLRP3	NACHT, LRR and PYD domains-containing protein 3
AMPK	AMP-activated protein kinase	PCR	polymerase chain reaction
ANOVA	analysis of variance	PFA	paraformaldehyde
AP	alkaline phosphatase	PGH1	prostaglandin G/H synthase 1
ASK1	apoptosis signal-regulating kinase 1	PGH2	prostaglandin G/H synthase 2
AST	aspartate aminotransferase	RNA	ribonucleic acid
BSA	bovine serum albumin	ROS	reactive oxygen species
CBA	chicken beta actin	SEM	standard error of the mean
DIO	diet-induced obesity	STZ	streptozotocin
DNA	deoxyribonucleic acid	T1DM	type 1 diabetes mellitus
GAPDH	glyceraldehyde-3-phosphate dehydrogenase	T2DM	type 2 diabetes mellitus
GTT	glucose tolerance test	TRX1	thioredoxin 1
HFD	high-fat, high-calorie diet;	TRX2	thioredoxin 2
HDL:	high-density lipoprotein	TXNIP	thioredoxin-interacting protein
L1	mouse line 1	VDUP1	vitamin D3 upregulated protein
LDH	lactate dehydrogenase		

a negative feedback loop, promotes caspase 3 cleavage and beta cell death (Saxena et al., 2010). In addition, obesity-induced insulin resistance with increased plasma glucose concentration was associated with overexpression of TXNIP. Hereby, TXNIP favors as a pro-apoptotic factor the death of beta cells (Szpigel et al., 2018). Furthermore, in human skeletal muscle TXNIP is involved in insulin-dependent and independent regulatory mechanisms of glucose uptake and its deletion reduces the production of glucose in the liver (Chutkow et al., 2008; Parikh et al., 2007). The kinase AMP-activated protein kinase (AMPK) phosphorylate TXNIP and thereby induce the uptake of glucose into the cells (Waldhart et al., 2017; Wu et al., 2013). Increased TXNIP expression has been recognized in diabetic neuropathy and associated with oxidative damage to the nerves (Price et al., 2006). In addition to glucose, endoplasmic reticulum stress was recognized as another cause of overexpression of TXNIP (Oslowski et al., 2012). Until today, it remains unknown whether TXNIP increase is a consequence or cause of diabetes (Shalev, 2014).

In summary, TXNIP plays an important role in a wide variety of biological processes, including proliferation, apoptosis, fatty acid and glucose metabolism, inflammation, and cancer (Forred et al., 2016; Spindel et al., 2012). In this study, a CBA^{TXNIP/+} transgenic mouse model was generated and employed to analyze the consequences of ubiquitous TXNIP overexpression. In light of the presumed effects of TXNIP in beta cell physiology, we assessed the consequences of its overexpression in glucose and energy metabolism parameters by applying a diet-induced obesity (DIO) model and a streptozotocin-induced T1DM model.

2. Materials and methods

2.1. Transgene construction

The *Txnip*-coding sequence was amplified from a murine cDNA pool by high-fidelity PCR (Phusion, New England Biolabs, Ipswich, MA, USA) using the following primers: m*Txnip_FW*: 5'-ACGGAGGCGAGCTCTTCG-3' and m*Txnip_REV*: 5'-GTCTCTGAAACACTGGAGTTCAAGC-3'. The amplicon was inserted into the StrataClone blunt cloning vector (Agilent, Munich, Germany), released as an *EcoRI* fragment and cloned downstream of the cytomegalovirus enhancer with chicken beta actin promoter, and upstream of a rabbit beta-globin 3'-flanking region with polyadenylation signal in the expression vector pUC-CAGGS (Schneider et al., 2005). Orientation and amplification fidelity were checked by Sanger sequencing using the primer pTORUseq: 5'-CTA-CAGCTCCTGGGCAACGTG-3'. The microinjection fragment was released from the vector backbone by *Sal*I and *Hind*III double digestion.

2.2. Mice

C57BL/6N and NMRI mice were purchased from Janvier (France) and maintained under specific-pathogen-free conditions in the closed barrier facility of the Gene Center Munich at 23 °C, 40% humidity and with a 12 h light/dark cycle (lights on at 7 a.m.). All mice had access to water and standard rodent diet (V1534; Ssniff, Soest, Germany) ad libitum, if not otherwise described. The injection fragment (diluted to 1.5 ng/µl) was microinjected into the pronucleus of C57BL/6N zygotes. Afterwards the manipulated zygotes were transplanted into pseudopregnant NMRI recipient females, which serve as excellent foster mothers. Three founders (CBA^{TXNIP/+}) were identified by PCR analysis and mated to wild-type C57BL/6N animals. Genomic DNA was isolated from tail clips using the Wizard DNA Extraction Kit (Clontech). Routine identification of transgenic mice was done by PCR using the primers pTORUseq: 5'-CTACAGCTCCTGGGCAACGTG-3' and Txnip_REV: 5'-ATCACCATCTCGTTCTCACC-3'. All mouse experiments were approved by the Committee of Animal Health and Care of the local governmental body of the state of Upper Bavaria (Regierung von Oberbayern), Germany, and were performed in strict compliance with the European Communities Council Directive (86/609/EEC) recommendations for the care and use of laboratory animals (55.2-1-54-2532-24-2017).

2.3. RNA expression analysis

Tissue samples were homogenized in TRIzol (Invitrogen, Karlsruhe, Germany) for RNA isolation, and 1 μg of RNA was reverse transcribed in a final volume of 40 μl using RevertAidreverse transcriptase (Thermo Scientific, Schwerte, Germany) according to the manufacturer's instructions. For qualitative mRNA expression of murine Txnip, reverse transcription-PCR (RT-PCR) using reagents from Qiagen (Hilden, Germany) was performed. The final reaction volume was 20 μl , and cycle conditions were 94 °C for 5 min followed by 35 cycles of 94 °C for 1 min, 60 °C for 1 min, and 72 °C for 1 min. The primers employed were m<code>Txnip_FW</code>, m<code>Txnip_REV</code>, <code>Gapdh</code> forward primer 5'-TCATCAACGG-GAAGCCCATCAC-3' and <code>Gapdh</code> reverse primer 5'-AGACTCCACGACA-TACTCAGCACCG-3'.

2.4. Western blot

Protein was extracted from mouse tissue using Laemmli-extraction-buffer. The protein concentrations were estimated via biochinin acid assay and 20 μg protein was separated by SDS-PAGE on a 10% gel. The protein was transferred to membranes (Immoblion-P Membran, Merck,

Darmstadt, Germany) by semidry blotting and was blocked in 5% milk (milk powder Roth, Karlsruhe, Germany). Primary antibodies were incubated in 2.5% BSA overnight at 4 °C. Used antibodies are listed in Table S3. After incubation the membranes were washed four times in TBS-T and then they were incubated in 5% BSA with a horseradish peroxidase-labeled secondary antibodies for 1 h at room temperature. For visualization of the bands an enhanced chemiluminescence detection reagent (ECL Advance Western Blotting Detection Kit, GE Healthcare) and appropriate x-ray films (GE Healthcare) were used. The membranes were stripped after detection with elution buffer (2% SDS, 6.25 mM Tris-HCl, pH 6.7 and 100 mM beta-mercaptoethanol) for 40 min at 70 °C and incubated with an antibody recognizing an appropriated reference protein. The Image Quant software package (GE Healthcare) was used to quantify the band intensities.

2.5. Blood chemistry

Blood was collected retro-orbitally in lithium-heparin tubes (KABE, Numbrecht-Elsenroth, Germany) under inhalation anesthesia. The tubes were centrifuged twice for 10 min at $2000\times g$ at 4 °C and the plasma samples were transferred to new plain sample tubes and stored at -80 °C until needed. Before analysis, samples were thawed at 4 °C, thoroughly mixed using a Vortex mixer and afterwards centrifuged for 10 min at $5000\times g$ and 8 °C to move clots to the bottom of the tube. Dependent on plasma volume obtained, plasma samples were either directly analyzed for clinical chemistry parameters, or after 1:2 dilution with deionized water. Parameters were measured using an AU480 autoanalyzer (Beckman Coulter, Krefeld, Germany) and adapted test kits provided by Beckman Coulter as previously described (Rathkolb et al., 2013).

2.6. Intraperitoneal glucose tolerance test

Briefly, for glucose tolerance test (GTT) mice were starved for 6 h in individual cages. A glucose bolus (1.5 mg/kg body weight) was injected intraperitoneally and blood samples were taken from the punctured tail vein at 0, 20, 40, 60, 80, 100, and 120 min after glucose injection and were immediately measured using a glucometer (FreeStyle Precision Neo, Abbott Diabetes Care, Wiesbaden, Germany) (Dahlhoff et al., 2014).

2.7. Diet-induced obesity

For diet-induced obesity (DIO) 8 female C57BL/6N control mice and 8 CBA $^{\rm TXNIP/+}$ transgenic female mice at 10 weeks of age were housed individually and received two weeks later for 10 weeks the D12492 high-fat, high-calorie diet (HFD) (E15741-34; Ssniff, Soest, Germany) ad libitum. Body weight was measured every week and food intake during the trial was monitored by weighing and re-weighing the feed every week. Food spilling could not be observed or detected in any cage. At the end of the DIO experiment, an intraperitoneal GTT was performed. Finally, the mice were sacrificed and organs were snap frozen at $-80\,^{\circ}\mathrm{C}$ or fixed in 4% paraformaldehyde (PFA, pH 7.4) for histology analysis.

2.8. Streptozotocin-induced diabetes

Streptozotocin (100 mg/kg body weight) was injected intraperitoneally in eight-week-old female mice and blood glucose levels were measured every 12 h with a glucometer (FreeStyle Precision Neo). Blood was taken from a punctured tail vein. Finally, mice were sacrificed after 7 days, blood was collected retro-orbitally under inhalation anesthesia, the pancreas was extracted immediately and snap frozen at $-80\,^{\circ}\mathrm{C}$ or fixed in 4% paraformaldehyde (PFA, pH 7.4) for histology analysis.

2.9. Histology and immunohistochemistry

Pancreas samples were embedded in paraffin and sections were

routinely stained by H&E as described previously (Hoesl et al., 2018). Beta cells were detected by immunohistochemistry as described previously (Dahlhoff et al., 2009). Tissue sections with 4 μm thickness were deparaffinized, rehydrated, and boiled for antigen retrieval for 20 min in a microwave at 95 °C in 10 mM sodium citrate buffer pH 6.0. After the slides were cooled down to room temperature, they were incubated in 3% H₂O₂ for 15 min for blocking the endogenous peroxidase, and afterwards blocked in rabbit serum (1:20 diluted in TBS-T). The sections were incubated with primary antibody (polyclonal guinea pig anti-insulin, P01315, Dako, Hamburg, Germany, 1:5000 dilution) for 1h at room temperature, followed by an incubation with a secondary antibody (rabbit anti-guinea pig Immunoglobulins/HRP, P0141, Dako, 1:500 dilution) for 1h at room temperature. 3,3'-diaminobenzidine (DAB) (Sigma, Taufkirchen, Germany) was used as the chromogen and the immunolabeled sections were counterstained with hematoxylin. Control experiments included the omission of the first antibody; all controls showed no DAB staining. Quantitative stereological analyses of the pancreas for calculating the beta cell volume were performed as described elsewhere in detail (Dahlhoff et al., 2009). Briefly, six sections evenly distributed throughout the whole pancreas were obtained from each animal and evaluated for morphometry. The pancreas was scanned in a meandering pattern with a visual frame and every tenth visual field was evaluated. The cross-sectional area of the pancreas was determined planimetrically by circling the immunohistochemically-stained sections by circling their contours with a cursor on the digitizing image analysis system of a Leica software (LAS V4.5., Leica, Wetzlar). In addition, the cross-sectional area of the beta cell profiles was measured. The volume of pancreas $(V_{(Pan)})$ before embedding was calculated by dividing the organ weight by the specific weight of mouse pancreas (1.08mg/mm3 (Wanke et al., 1994)). The volume density of the beta cells in the pancreas ($V\nu_{(Beta\ cells/Pan)}$) was calculated by dividing the sum of cross-sectional areas of all beta cell profiles by the sum of the cross-sectional areas of the pancreas. The total beta cell volume ($V_{(Beta\ cell/Pan)}$) was calculated by multiplying the $V\nu_{\text{(Beta cell/Pan)}}$ by $V_{\text{(Pan)}}$.

2.10. Statistical analysis

Data are presented as mean \pm SEM and compared by Student's *t*-test (GraphPad Prism version 5.0 for Windows, GraphPad Software, San Diego, CA, USA), and in the case of more than two groups by analysis of variance (ANOVA) and Tukey's multiple comparison test. GTT and STZ-experiments were analyzed by 2-way ANOVA. Group differences were considered to be statistically significant if P < 0.05.

3. Results

3.1. Ubiquitous overexpression of TXNIP has no evident phenotypical consequences

Txnip transcripts are expressed in nearly all tissues and organs in mice, as shown by RT-PCR (Fig. S1A). Due to the ubiquitous expression of TXNIP, we decided to investigate TXNIP in a gain of function mouse model by placing the Txnip cDNA under control of the chicken-betaactin promoter to overexpress TXNIP widely. Three TXNIPoverexpressing mouse lines (CBA^{TXNIP/+}, L1, L2, and L3) were generated by DNA microinjection and the transgenic animals were identified by PCR analysis (Fig. S1B). The TXNIP expression levels of all three mouse lines were determined in various organs (pancreas, salivary gland, kidney, ovary, uterus, and liver) by Western blot analysis. As mice from line L3 showed the strongest TXNIP expression in the pancreas (Fig. S1C and Fig. 1A), and no macroscopical or histological changes were observed in any of the transgenic lines (data not shown). All further experiments were done with female mice of line 3, if not described otherwise. Body weight of male and female mice were measured over 10 weeks and revealed no alterations between transgenic and control

littermates in both sexes (Fig. 1B and C). Plasma cholesterol, glucose, low-density lipoprotein (LDL), high-density lipoprotein (HDL), bilirubin, and albumin were also unaltered in female transgenic CBA TXNIP/+ mice compared to control mice (Fig. 1E). To assess inflammation of the liver and pancreas, several specific enzymes were investigated in the plasma of CBA^{TXNÍP/+} and control mice. Aspartate aminotransferase (AST), alanine aminotransferase (ALT), and alkaline phosphatase (AP) were measured to determine liver damage, but no differences were detected between both groups (Fig. 1F). Furthermore, no changes were detected in the enzymes lactate dehydrogenase (LDH), lipase, and alphaamylase, which are usually increased in pancreatitis (Fig. 1F). Fasted plasma insulin levels were not altered in transgenic $CBA^{TXNIP/+}$ mice compared to controls (Fig. 1D), further indicating that the overexpression of TXNIP did not affect beta cell function. Lactate is the final product of anaerobic glycolysis and increased lactate levels may indicate hypoxia. However, plasma lactate levels were unchanged in the transgenic CBA^{TXNIP/+} mice compared to controls (Fig. 1G).

3.2. TXNIP overexpression does not influence diet-induced obesity

To challenge the regulation of blood glucose level and associated metabolic processes, mice were fed for 10 weeks with a high-fat diet. The increase in diet-induced body weight (Fig. 2A and B) and absolute and relative food intake (Fig. 2C and D) in CBA^{TXNIP/+} mice did not differ from those of control littermates. There were also no differences in the absolute and relative abdominal, subcutaneous, or brown fat depot weights of $CBA^{TXNIP/+}$ mice compared with controls (Fig. 2E and F). In addition, no alterations were found in the weight of pancreas, spleen, and liver of CBATXNIP/+ animals (Fig. 2E and F). At the end of the experiment, neither plasma insulin levels (Fig. 2G) were altered in obese transgenic CBA^{TXNIP/+} mice compared to obese controls, nor changes between both groups of mice were detected in a glucose tolerance test (Fig. 2H). In contrast, comparison of GTT data of lean mice with obese mice, independently of their TXNIP status, showed clearly that the fasted glucose levels during GTT of obese mice were significantly different from lean mice: blood glucose levels were significantly increased in both DIO groups compared to lean groups, suggesting onset of a T2DM-like

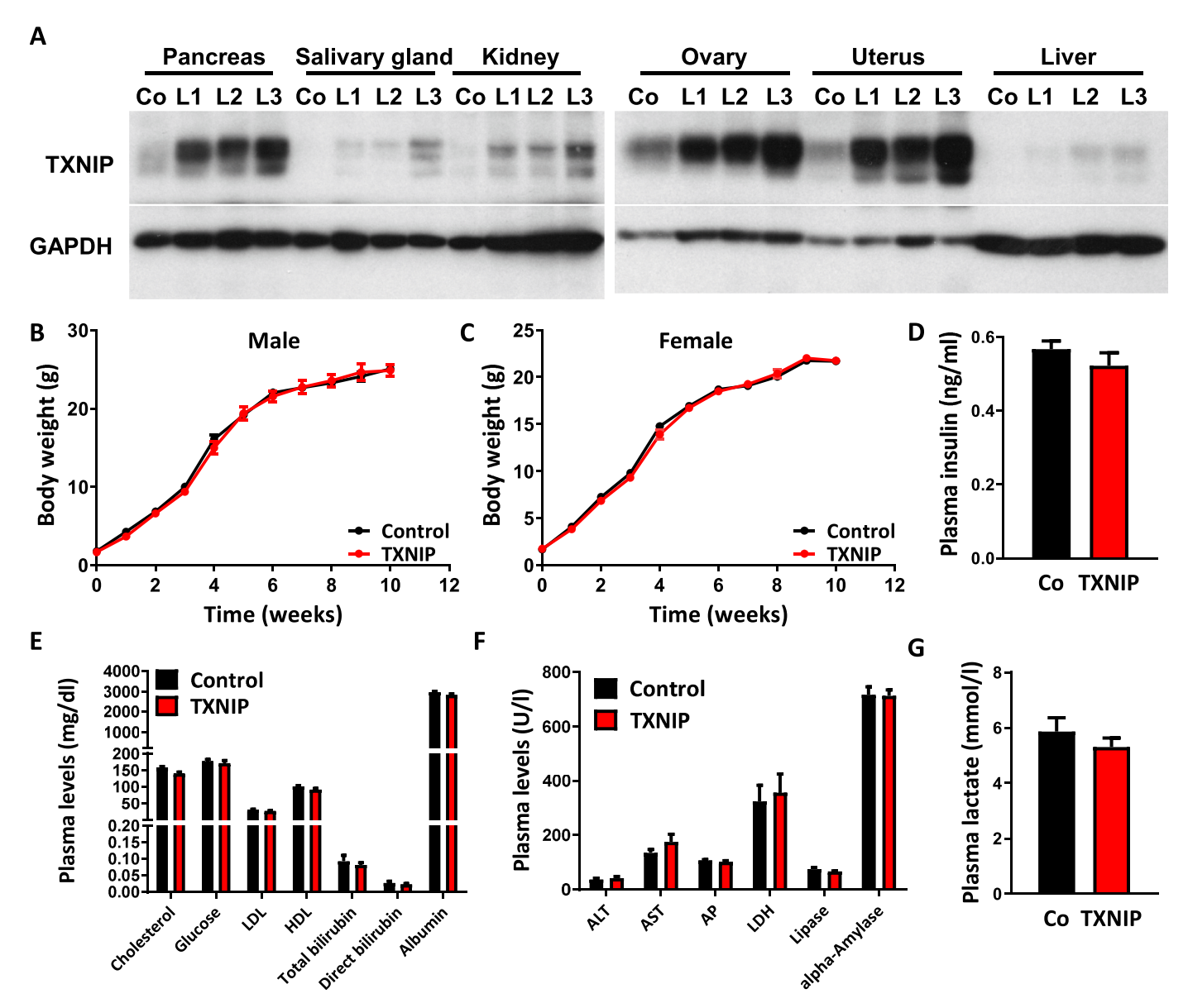


Fig. 1. (A) Western blot analyses of TXNIP expression in several organs from female mice of all three (L1, L2, L3) transgenic mouse lines. GAPDH was used as reference protein. (B–C) Body weight of (B) male (n = 6) and (C) female (n = 5) CBA^{TXNIP/+} transgenic mice and control littermates. (D–G) Plasma levels of several enzymes and substrates demonstrating no differences between eight weeks old transgenic and control female mice (n = 6).

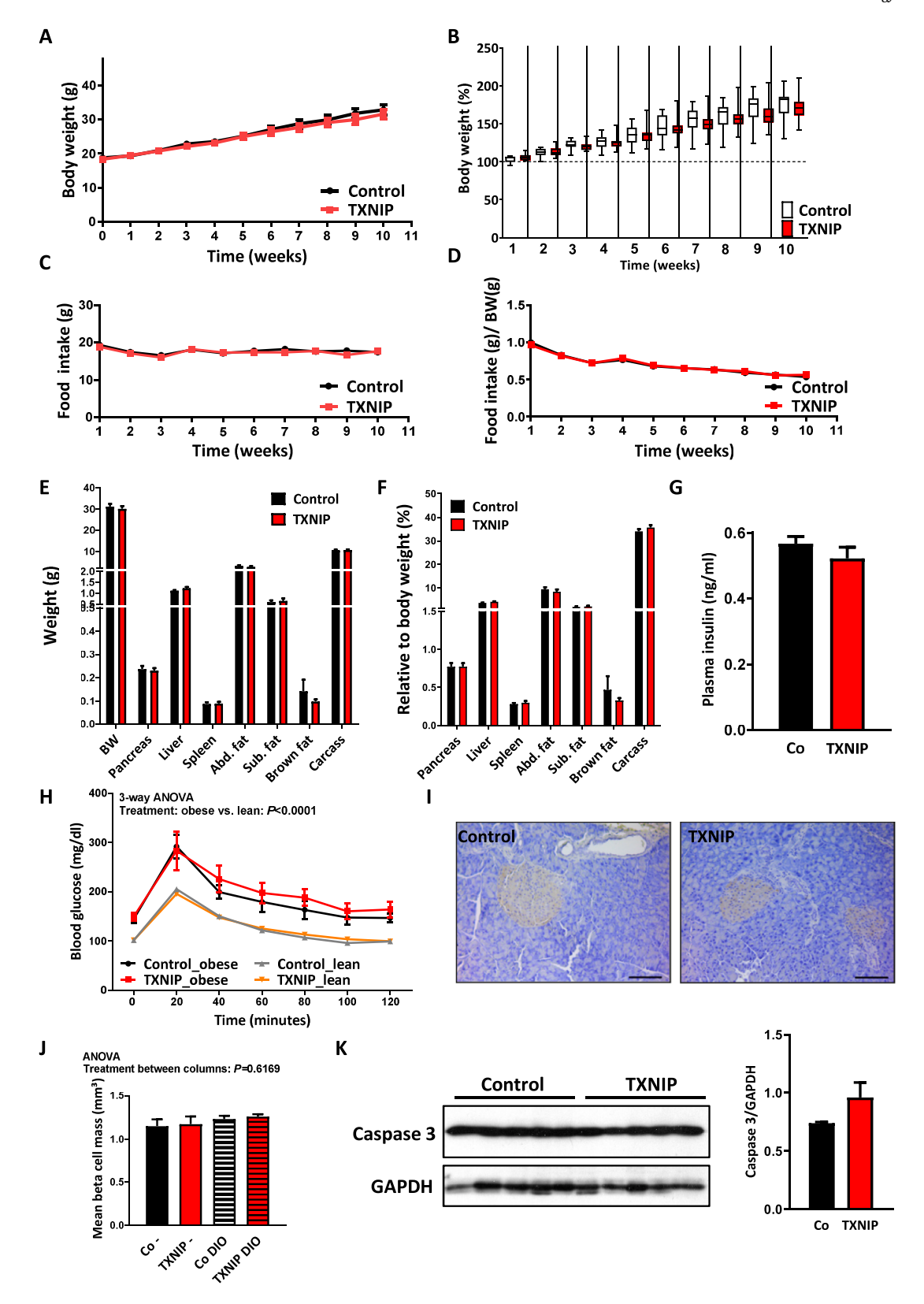


Fig. 2. (A) Body weight curve of female CBA^{TXNIP/+} mice and controls under HFD (n = 8). (B) Body weight normalized to starting body weight (n = 8). (C) Individual weekly food intake (n = 8). (D) Individual weekly food intake normalized to body weight (n = 8). (E) Absolute and (F) relative tissue weights from female CBA^{TXNIP/+} mice and control animals (n = 7). (G) Plasma insulin measurements of fasted obese female CBA^{TXNIP/+} mice compared with controls (n = 4). (H) Intraperitoneal GTT of female lean and obese CBA^{TXNIP/+} mice and control littermates (n = 6). Data were analyzed by 3-way ANOVA and are represented as means \pm SEM. (I) Representative immunohistochemistry staining for insulin in female CBA^{TXNIP/+} transgenic mice and control littermates. Scale bars represent 100 μ m. (J) Morphometrical analysis of the mean beta cell mass of female CBA^{TXNIP/+} mice and controls fed with maintenance diet (–) and female CBA^{TXNIP/+} mice and controls under DIO (+) (n = 6). Data are represented as means \pm SEM and were analyzed by treatment between columns with one-way ANOVA (P = 0.6169). (K) Western blot analyses of caspase 3 expression in the pancreas of obese female transgenic mice and controls. GAPDH was used as reference protein. All data were analyzed by Student's t-test and are presented as means \pm SEM.

phenotype in the overweight animals (Fig. 2H). Histological examination and stereological analysis of beta cell mass within endocrine islets of pancreas sections stained for insulin showed no alterations between transgenic and control animals (Fig. 2I and J). Finally, we examined the obese mice for apoptosis in the pancreas, but could not detect cleaved caspase 3 in the pancreas of the transgenic CBA^{TXNIP/+} or control animals (Fig. 2K).

3.3. Overexpression of TXNIP overproportionally reduces beta cell mass and increases blood glucose levels after streptozotocin treatment

A single high-dose of streptozotocin was injected intraperitoneally to induce diabetes in $CBA^{TXNIP/+}$ and control mice. $CBA^{TXNIP/+}$ mice developed significant higher blood glucose levels compared to control littermates (Fig. 3A). In addition, a GTT revealed significant increased

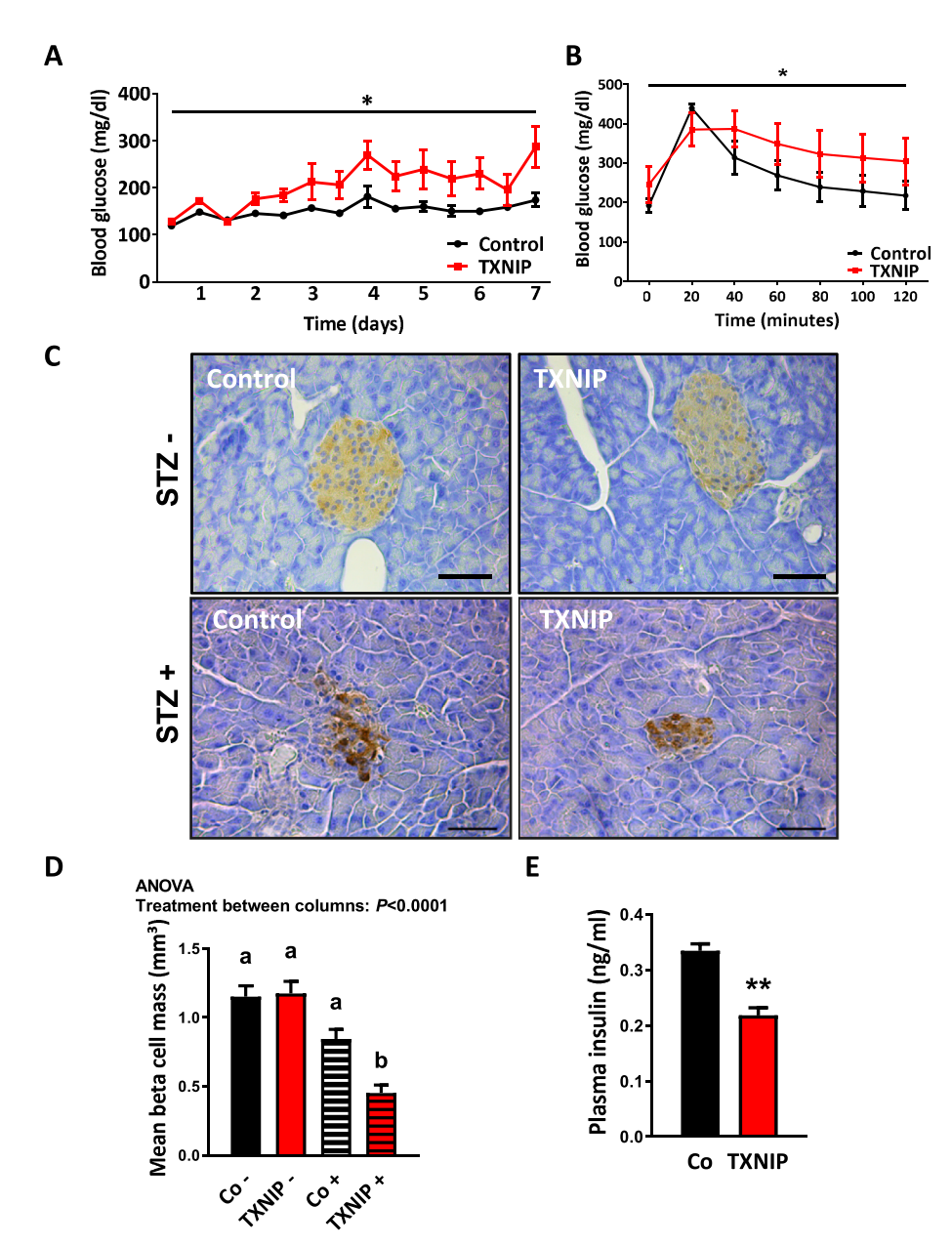


Fig. 3. (A) Glucose levels of female CBATXNIP/+ transgenic and control mice after streptozotocin application (n = 6). Data were analyzed by 2-way ANOVA and are represented as means ± SEM. Significant genotype \times time interaction: *P < 0.05. (B) Intraperitoneal GTT of female CBA^{TXNIP/+} mice and control littermates (n = 6). Data were analyzed by 2way ANOVA and are represented as means \pm SEM. Significant genotype \times time interaction: *P < 0.05. (C) Representative immunohistochemistry stainings against insulin before (STZ -) and after (STZ +) streptozotocin treatment of female $CBA^{TXNIP/+}$ transgenic and control mice. (D) Morphometrical analysis of the mean beta cell mass of untreated (-) and streptozotocin treated (+) female $CBA^{TXNIP/+}$ mice compared with controls (n = 6). Data are represented as means \pm SEM and were analyzed by treatment between columns with one-way ANOVA (P < 0.0001) and each group with each group by Student's t-test (b is significantly different from a, P < 0.001). (E) Plasma insulin measurements of streptozotocin treated female CBATXNIP/+ mice compared with controls (n = 6). Data were analyzed by Student's t-test and are represented as means \pm SEM. *P < 0.05.

blood glucose levels in transgenic CBA $^{TXNIP/+}$ mice compared with controls (Fig. 3B). Immunohistochemical staining for insulin confirmed reduced beta cell mass in the pancreatic endocrine islets of both CBA $^{TXNIP/+}$ and control mice after streptozotocin treatment (Fig. 3C). Morphometric analysis revealed that the mean beta cell mass was unchanged between groups in the absence of streptozotocin treatment (Fig. 3D), thus confirming our previous observation in obese mice (Fig. 2J). In contrast, beta cell mass was significantly reduced in CBA $^{TXNIP/+}$ mice compared with control littermates after streptozotocin

treatment (Fig. 3D). Additionally, the plasma insulin levels of strepto-zotocin treated CBA^{TXNIP/+} mice were significantly reduced compared to control mice (Fig. 3E). These findings demonstrate that the beta cells of transgenic animals were more severely damaged compared to the beta cells of controls. These results correspond well to the previous data of the blood glucose measurements and GTT. In summary, the over-expression of TXNIP enhances the toxic effect of streptozotocin in beta cells and increases the severity of streptozotocin-induced diabetes.

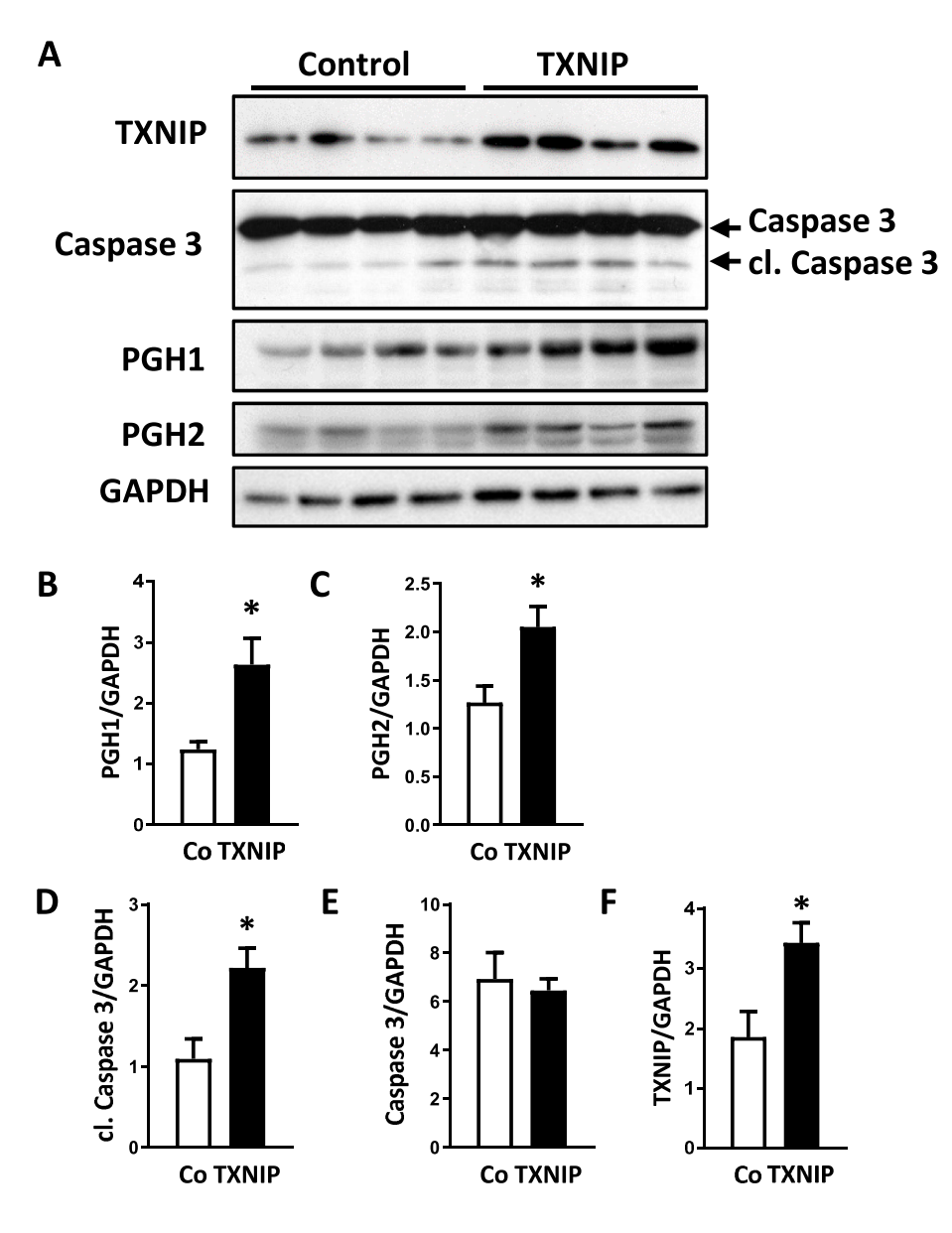


Fig. 4. (A) Western blot analyses of TXNIP, Caspase3, PGH1, and PGH2 expression in the pancreas of streptozotocin treated female CBA^{TXNIP/+} transgenic mice and control littermates. GAPDH was used as reference protein. (B–F) The expression of (B) PGH1, (C) PGH2, (D) cleaved caspase 3, and (F) TXNIP were significantly increased in the pancreas of streptozotocin treated female CBA^{TXNIP/+} transgenic mice compared to controls, but not for (E) uncleaved caspase 3 (n = 4). Data were analyzed by Student's *t*-test and are represented as means \pm SEM. *P < 0.05.

3.4. PGH1 and PGH2 are increasedly expressed in the pancreas of $CBA^{TXNIP/+}$ transgenic mice

Since prostaglandin G/H synthase 1 and 2 (PGH1, PGH2) play a role in inflammatory responses, and PGH2 was associated with streptozotocin-induced beta cell damage (Perrone et al., 2009, 2010), the expression of both proteins was investigated by Western blot to determinate their potential involvement in the inflammatory effect of streptozotocin (Fig. 4A). Densitometric analysis revealed an increased expression of PGH1 and PGH2 proteins in the pancreas of CBA^{TXNIP/+} mice compared to control littermates (Fig. 4B and C). Apoptosis, assessed by Western blots, showed significantly increased abundance of active (cleaved) caspase 3 in transgenic CBA^{TXNIP/+} mice compared to controls (Fig. 4D), but not for inactive (uncleaved) caspase 3 (Fig. 4E).

Although we assessed whole pancreatic tissue in our analysis, these results additionally support the observation that streptozotocin has a stronger damaging effect on pancreatic beta cells of $CBA^{TXNIP/+}$ transgenic mice compared to control animals. A Western blot for TXNIP confirmed significantly higher levels of TXNIP in the pancreas of transgenic mice compared to controls in streptozotocin-treated mice (Fig. 4F).

4. Discussion

In this study, we aimed to investigate the effects of TXNIP in a mouse model that overexpresses this protein ubiquitously. TXNIP is an alphaarrestin protein, whose transcripts are expressed in nearly all organs and tissues, which we also confirmed in this study. Although TXNIP is a critical regulator of energy metabolism, several details on the mechanism by which TXNIP acts on molecular level remain unknown, and the CBA $^{\rm TXNIP}/+$ transgenic mouse model could be helpful to clarify these open questions.

It is assumed that TXNIP acts as a switch between glucose toxicity and beta cell apoptosis, whereby insulin resistance or diabetes with high blood glucose levels increase TXNIP expression (Minn et al., 2005a). TXNIP knockout mice showed increased beta cell volume and increased insulin level with decreased blood glucose levels and improved glucose tolerance tests. In a DIO model TXNIP knockout mice showed improved glucose tolerance and increased insulin sensitivity under HFD compared to controls (Lei et al., 2022). These results indicate that the loss of TXNIP is connected to beta cell proliferation and insulin production, and diabetes seems to be related with TXNIP overexpression in beta cells. CBA^{TXNIP/+} mice showed no alterations in blood glucose levels, plasma insulin levels or in beta cell volume, suggesting that increased TXNIP levels alone do not cause beta cell apoptosis and elevated blood glucose levels. As one of the most common risk factors for T2DM is obesity, we used DIO to assess TXNIP effects on beta cell apoptosis under an additional trigger. CBATXNIP/+ mice and control littermates fed with HFD developed obesity, and a glucose tolerance test showed hyperglycemia in both groups as expected. Furthermore, the transgenic animals showed no alterations in beta cell mass, beta cell morphology, or glucose levels compared with controls. Contrary to our expectation, the obese phenotype did not lead to any detectable increase in beta cell apoptosis due to increased TXNIP expression in the transgenic mice. TXNIP knockout mice receiving a high fat diet showed also no changes in weight gain compared to control mice (Elshaer et al., 2017). Thus, overexpression of TXNIP alone is not sufficient to alter beta cells, drive them into apoptosis, and cause high blood glucose levels. However, in a streptozotocin-induced T1DM model, transgenic mice showed a more severe diabetic phenotype and significantly higher blood glucose levels than their littermates. Thus, the severity by which streptozotocin damages beta cells is strongly influenced by the overexpression of TXNIP.

TXNIP also frequently interacts with NLRP3 in a ROS-dependent manner and could activate the NLRP3 inflammasome (Zhou et al., 2010). TXNIP and NLRP3 knockout mice have a similar phenotype showing alterations in blood glucose concentrations, insulin secretion,

and insulin sensitivity (Chen et al., 2008a; Hui et al., 2008; Oka et al., 2009; Zhou et al., 2010). Although TXNIP overexpression may drive inflammations, we did not find histological inflammation foci in any tissue or organ in CBA^{TXNIP/+} mice. Blood marker enzymes for hepatitis or pancreatitis were not increased in CBA^{TXNIP/+} mice compared with controls. However, in the pancreas of CBA^{TXNIP/+} mice treated with streptozotocin we detected increased levels of PGH2 and PGH1, showing enhanced oxidative stress as it was shown in TXNIP-induced diabetic retinopathy (Perrone et al., 2009; Perrone et al., 2010). Besides, hyperglycemia-induced TXNIP overexpression was associated with an inflammatory response resulting in an increased PGH expression (Kumar and Mittal, 2018). However, as the pancreas of CBA TXNIP/+ mice showed increased apoptosis after treatment with streptozotocin, these results are in line with previous studies showing that TXNIP could induces apoptosis via ASK1 activation (Chen et al., 2008a; Chen et al., 2008b; Minn et al., 2005a). Most results of our study are based on female mice, which represents a clear limitation, as there may be differences in glucose metabolism or obesity development between females and males and it could not be excluded that male CBATXNIP/+ mice would have responded differently to the DIO or streptozotocin experiments.

TXNIP could acts as a tumor suppressor in many cancer types, including osteosarcoma (Yuan et al., 2022), breast cancer (Okumura et al., 2021) or acute myeloid leukemia (Noura et al., 2020), making it a highly interesting target for cancer therapies (Qayyum et al., 2021). The newly generated CBA $^{\rm TXNIP/+}$ transgenic mouse line will be suitable for addressing the role of TXNIP in cancer research, as it can be used to study the function of TXNIP in detail in different carcinogen- or oncogene-induced tumors very easily, and to analyze TXNIP as a potential target for new cancer therapies.

5. Conclusion

In conclusion, our results unexpectedly show that an increased TXNIP expression alone has no effect on pancreatic beta cell mass and glucose metabolism. In addition, hyperglycemia caused by high fat diet had no detrimental effect on beta cells of the transgenic mice. In contrast, overexpression of TXNIP overproportionally reduced beta cell mass in a streptozotocin-induced T1DM model and impaired glucose regulation, thus increasing the severity of the disease.

Availability of data and materials

All data generated or analyzed during this study are included in this published article and its supplementary information files.

Funding information

Not applicable.

CRediT authorship contribution statement

Marlon R. Schneider: Conceptualization, Data curation, Formal analysis, Writing – original draft, of the manuscript, Project administration, Supervision, Writing – review & editing. Silja Zettler: Acquisition of data, Writing – original draft, of the manuscript, Statistical analysis, Project administration. Birgit Rathkolb: Acquisition of data, Writing – original draft, of the manuscript, Project administration. Maik Dahlhoff: Conceptualization, Data curation, Formal analysis, Writing – original draft, of the manuscript, Statistical analysis, Project administration, Supervision, Writing – review & editing.

Declaration of competing interest

The authors declare that they have no conflict of interest.

Data availability

Data will be made available on request.

Acknowledgments

We thank Dr. Ingrid Renner-Müller and Petra Renner for excellent animal care, Maximillian Marschall and Franziska Kress for assistance with Western blot analysis, Sebastian Kaidel for mouse plasma analyses, and Josef Millauer for mouse genotyping.

Appendix A. Supplementary data

Supplementary data to this article can be found online at https://doi.org/10.1016/j.mce.2023.111885.

References

- Chen, J., Cha-Molstad, H., Szabo, A., Shalev, A., 2009. Diabetes induces and calcium channel blockers prevent cardiac expression of proapoptotic thioredoxin-interacting protein. Am. J. Physiol. Endocrinol. Metab. 296, E1133–E1139.
- Chen, J., Hui, S.T., Couto, F.M., Mungrue, I.N., Davis, D.B., Attie, A.D., Lusis, A.J., Davis, R.A., Shalev, A., 2008a. Thioredoxin-interacting protein deficiency induces Akt/Bcl-xL signaling and pancreatic beta-cell mass and protects against diabetes. Faseb. J. 22, 3581–3594.
- Chen, J., Saxena, G., Mungrue, I.N., Lusis, A.J., Shalev, A., 2008b. Thioredoxininteracting protein: a critical link between glucose toxicity and beta-cell apoptosis. Diabetes 57, 938-944.
- Chen, K.S., DeLuca, H.F., 1994. Isolation and characterization of a novel cDNA from HL-60 cells treated with 1,25-dihydroxyvitamin D-3. Biochim. Biophys. Acta 1219, 26–32.
- Chutkow, W.A., Patwari, P., Yoshioka, J., Lee, R.T., 2008. Thioredoxin-interacting protein (Txnip) is a critical regulator of hepatic glucose production. J. Biol. Chem. 283, 2397–2406.
- Dahlhoff, M., Dames, P.M., Lechner, A., Herbach, N., van Burck, L., Wanke, R., Wolf, E., Schneider, M.R., 2009. Betacellulin overexpression in transgenic mice improves glucose tolerance and enhances insulin secretion by isolated islets in vitro. Mol. Cell. Endocrinol. 299, 188–193.
- Dahlhoff, M., Pfister, S., Blutke, A., Rozman, J., Klingenspor, M., Deutsch, M.J., Rathkolb, B., Fink, B., Gimpfl, M., Hrabė de Angelis, M., Roscher, A.A., Wolf, E., Ensenauer, R., 2014. Peri-conceptional obesogenic exposure induces sex-specific programming of disease susceptibilities in adult mouse offspring. Biochim. Biophys. Acta 1842, 304–317.
- Elshaer, S.L., Mohamed, I.N., Coucha, M., Altantawi, S., Eldahshan, W., Bartasi, M.L., Shanab, A.Y., Lorys, R., El-Remessy, A.B., 2017. Deletion of TXNIP Mitigates High-Fat Diet-Impaired Angiogenesis and Prevents Inflammation in a Mouse Model of Critical Limb Ischemia, vol. 6. Antioxidants, Basel).
- Forred, B.J., Neuharth, S., Kim, D.I., Amolins, M.W., Motamedchaboki, K., Roux, K.J., Vitiello, P.F., 2016. Identification of redox and glucose-dependent Txnip protein interactions. Oxid. Med. Cell. Longev., 5829063, 2016.
- Hoesl, C., Rohrl, J.M., Schneider, M.R., Dahlhoff, M., 2018. The receptor tyrosine kinase ERBB4 is expressed in skin keratinocytes and influences epidermal proliferation. Biochim. Biophys. Acta Gen. Subj. 1862, 958–966.
- Hui, S.T., Andres, A.M., Miller, A.K., Spann, N.J., Potter, D.W., Post, N.M., Chen, A.Z., Sachithanantham, S., Jung, D.Y., Kim, J.K., Davis, R.A., 2008. Txnip balances metabolic and growth signaling via PTEN disulfide reduction. Proc. Natl. Acad. Sci. U. S. A. 105, 3921–3926.
- Junn, E., Han, S.H., Im, J.Y., Yang, Y., Cho, E.W., Um, H.D., Kim, D.K., Lee, K.W., Han, P. L., Rhee, S.G., Choi, I., 2000. Vitamin D3 up-regulated protein 1 mediates oxidative stress via suppressing the thioredoxin function. J. Immunol. 164, 6287–6295.
- Kumar, A., Mittal, R., 2018. Mapping Txnip: key connexions in progression of diabetic nephropathy. Pharmacol. Rep. 70, 614–622.
- Lee, K.N., Kang, H.S., Jeon, J.H., Kim, E.M., Yoon, S.R., Song, H., Lyu, C.Y., Piao, Z.H., Kim, S.U., Han, Y.H., Song, S.S., Lee, Y.H., Song, K.S., Kim, Y.M., Yu, D.Y., Choi, I., 2005. VDUP1 is required for the development of natural killer cells. Immunity 22, 195–208.
- Lei, Z., Chen, Y., Wang, J., Zhang, Y., Shi, W., Wang, X., Xing, D., Li, D., Jiao, X., 2022. Txnip deficiency promotes β -cell proliferation in the HFD-induced obesity mouse model. Endocr Connect 11.
- Li, J., Yue, Z., Xiong, W., Sun, P., You, K., Wang, J., 2017. TXNIP overexpression suppresses proliferation and induces apoptosis in SMMC7221 cells through ROS generation and MAPK pathway activation. Oncol. Rep. 37, 3369–3376.
- Lu, J., Holmgren, A., 2012. Thioredoxin system in cell death progression. Antioxidants Redox Signal. 17, 1738–1747.
- Minn, A.H., Hafele, C., Shalev, A., 2005a. Thioredoxin-interacting protein is stimulated by glucose through a carbohydrate response element and induces beta-cell apoptosis. Endocrinology 146, 2397–2405.
- Minn, A.H., Pise-Masison, C.A., Radonovich, M., Brady, J.N., Wang, P., Kendziorski, C., Shalev, A., 2005b. Gene expression profiling in INS-1 cells overexpressing thioredoxin-interacting protein. Biochem. Biophys. Res. Commun. 336, 770–778.

- Nishiyama, A., Matsui, M., Iwata, S., Hirota, K., Masutani, H., Nakamura, H., Takagi, Y., Sono, H., Gon, Y., Yodoi, J., 1999. Identification of thioredoxin-binding protein-2/vitamin D(3) up-regulated protein 1 as a negative regulator of thioredoxin function and expression. J. Biol. Chem. 274, 21645–21650.
- Noura, M., Matsuo, H., Koyama, A., Adachi, S., Masutani, H., 2020. TXNIP induces growth arrest and enhances ABT263-induced apoptosis in mixed-lineage leukemiarearranged acute myeloid leukemia cells. FEBS Open Bio 10, 1532–1541.
- Oka, S., Yoshihara, E., Bizen-Abe, A., Liu, W., Watanabe, M., Yodoi, J., Masutani, H., 2009. Thioredoxin binding protein-2/thioredoxin-interacting protein is a critical regulator of insulin secretion and peroxisome proliferator-activated receptor function. Endocrinology 150, 1225–1234.
- Okumura, S., Hirano, Y., Komatsu, Y., 2021. Stable duplex-linked antisense targeting miR-148a inhibits breast cancer cell proliferation. Sci. Rep. 11, 11467.
- Oslowski, C.M., Hara, T., O'Sullivan-Murphy, B., Kanekura, K., Lu, S., Hara, M., Ishigaki, S., Zhu, L.J., Hayashi, E., Hui, S.T., Greiner, D., Kaufman, R.J., Bortell, R., Urano, F., 2012. Thioredoxin-interacting protein mediates ER stress-induced beta cell death through initiation of the inflammasome. Cell Metabol. 16, 265–273.
- Parikh, H., Carlsson, E., Chutkow, W.A., Johansson, L.E., Storgaard, H., Poulsen, P., Saxena, R., Ladd, C., Schulze, P.C., Mazzini, M.J., Jensen, C.B., Krook, A., Bjornholm, M., Tornqvist, H., Zierath, J.R., Ridderstrale, M., Altshuler, D., Lee, R.T., Vaag, A., Groop, L.C., Mootha, V.K., 2007. TXNIP regulates peripheral glucose metabolism in humans. PLoS Med. 4, e158.
- Perrone, L., Devi, T.S., Hosoya, K., Terasaki, T., Singh, L.P., 2009. Thioredoxin interacting protein (TXNIP) induces inflammation through chromatin modification in retinal capillary endothelial cells under diabetic conditions. J. Cell. Physiol. 221, 262–272.
- Perrone, L., Devi, T.S., Hosoya, K.I., Terasaki, T., Singh, L.P., 2010. Inhibition of TXNIP expression in vivo blocks early pathologies of diabetic retinopathy. Cell Death Dis. 1, e65.
- Price, S.A., Gardiner, N.J., Duran-Jimenez, B., Zeef, L.A., Obrosova, I.G., Tomlinson, D. R., 2006. Thioredoxin interacting protein is increased in sensory neurons in experimental diabetes. Brain Res. 1116, 206–214.
- Qayyum, N., Haseeb, M., Kim, M.S., Choi, S., 2021. Role of thioredoxin-interacting protein in diseases and its therapeutic outlook. Int. J. Mol. Sci. 22.
- Rathkolb, B., Hans, W., Prehn, C., Fuchs, H., Gailus-Durner, V., Aigner, B., Adamski, J., Wolf, E., Hrabě de Angelis, M., 2013. Clinical chemistry and other laboratory tests on mouse plasma or serum. Curr. Protoc. Mol. Biol. 3, 69–100.
- Saxena, G., Chen, J., Shalev, A., 2010. Intracellular shuttling and mitochondrial function of thioredoxin-interacting protein. J. Biol. Chem. 285, 3997–4005.
 Schneider, M.R., Dahlhoff, M., Herbach, N., Renner-Mueller, I., Dalke, C., Puk, O.,
- Schneider, M.R., Dahlhoff, M., Herbach, N., Renner-Mueller, I., Dalke, C., Puk, O., Graw, J., Wanke, R., Wolf, E., 2005. Betacellulin overexpression in transgenic mice causes disproportionate growth, pulmonary hemorrhage syndrome, and complex eye pathology. Endocrinology 146, 5237–5246.
 Shaked, M., Ketzinel-Gilad, M., Ariav, Y., Cerasi, E., Kaiser, N., Leibowitz, G., 2009.
- Shaked, M., Ketzinel-Gilad, M., Ariav, Y., Cerasi, E., Kaiser, N., Leibowitz, G., 2009. Insulin counteracts glucotoxic effects by suppressing thioredoxin-interacting protein production in INS-1E beta cells and in Psammomys obesus pancreatic islets. Diabetologia 52, 636–644.
- Shalev, A., 2014. Minireview: thioredoxin-interacting protein: regulation and function in the pancreatic beta-cell. Mol. Endocrinol. 28, 1211–1220.
- Sheth, S.S., Bodnar, J.S., Ghazalpour, A., Thipphavong, C.K., Tsutsumi, S., Tward, A.D., Demant, P., Kodama, T., Aburatani, H., Lusis, A.J., 2006. Hepatocellular carcinoma in Txnip-deficient mice. Oncogene 25, 3528–3536.
- Spindel, O.N., World, C., Berk, B.C., 2012. Thioredoxin interacting protein: redox dependent and independent regulatory mechanisms. Antioxidants Redox Signal. 16, 587–596.
- Szpigel, A., Hainault, I., Carlier, A., Venteclef, N., Batto, A.F., Hajduch, E., Bernard, C., Ktorza, A., Gautier, J.F., Ferre, P., Bourron, O., Foufelle, F., 2018. Lipid environment induces ER stress, TXNIP expression and inflammation in immune cells of individuals with type 2 diabetes. Diabetologia 61, 399–412.
- Waldhart, A.N., Dykstra, H., Peck, A.S., Boguslawski, E.A., Madaj, Z.B., Wen, J., Veldkamp, K., Hollowell, M., Zheng, B., Cantley, L.C., McGraw, T.E., Wu, N., 2017. Phosphorylation of TXNIP by AKT mediates acute influx of glucose in response to insulin. Cell Rep. 19, 2005–2013.
- Wanke, R., Weis, S., Kluge, D., Kahnt, D., Schenck, E., Brem, G., Herrmanns, W., 1994.
 Morphometric evaluation of the pancreas of growth hormone transgenic mice. Acta Stereol. 13, 3–8.
- Wu, N., Zheng, B., Shaywitz, A., Dagon, Y., Tower, C., Bellinger, G., Shen, C.H., Wen, J., Asara, J., McGraw, T.E., Kahn, B.B., Cantley, L.C., 2013. AMPK-dependent degradation of TXNIP upon energy stress leads to enhanced glucose uptake via GLUT1. Mol. Cell 49, 1167–1175.
- Xu, G., Chen, J., Jing, G., Shalev, A., 2013. Thioredoxin-interacting protein regulates insulin transcription through microRNA-204. Nat. Med. 19, 1141–1146.
- Ye, X., Zuo, D., Yu, L., Zhang, L., Tang, J., Cui, C., Bao, L., Zan, K., Zhang, Z., Yang, X., Chen, H., Tang, H., Zu, J., Shi, H., Cui, G., 2017. ROS/TXNIP pathway contributes to thrombin induced NLRP3 inflammasome activation and cell apoptosis in microglia. Biochem. Biophys. Res. Commun. 485, 499–505.
- Yoshihara, E., Masaki, S., Matsuo, Y., Chen, Z., Tian, H., Yodoi, J., 2014. Thioredoxin/ Txnip: redoxisome, as a redox switch for the pathogenesis of diseases. Front. Immunol. 4, 514.
- Yuan, Y., Liu, Q., Wu, Z., Zhong, W., Lin, Z., Luo, W., 2022. TXNIP inhibits the progression of osteosarcoma through DDIT4-mediated mTORC1 suppression. Am. J. Cancer Res. 12, 3760–3779.
- Zhou, R., Tardivel, A., Thorens, B., Choi, I., Tschopp, J., 2010. Thioredoxin-interacting protein links oxidative stress to inflammasome activation. Nat. Immunol. 11, 136–140.